Folding-model description of elastic and inelastic scattering of ^{9}Be by ^{40,44}Ca and ^{39}K at 40 MeV

V. Hnizdo,* J. Szymakowski, K. W. Kemper, and J. D. Fox
Department of Physics, Flordia State University, Tallahassee, Florida 32306
(Received 24 March 1981)

Angular distributions have been measured for elastic scattering of ^{9}Be + ^{40,44}Ca and ^{9}Be + ^{39}K at $E_{lab} = 40$ MeV, covering an angular range up to $\theta_{c.m.} = 120°$ ($\sigma/\sigma_R \simeq 10^{-5}$), and for inelastic scattering of ^{9}Be leading to the first 2^+, 3^-, and 5^- states in ^{40}Ca, and the first 2^+ state in ^{44}Ca. The large angle cross sections ($\theta_{c.m.} = 173°$) measured are an order of magnitude smaller than those reported earlier for ^{6}Li scattering in this mass region. The data are analyzed in terms of the double-folding model with a realistic effective nucleon-nucleon interaction. The need to renormalize the effective interaction by a factor of ~ 0.6 is removed when the strong projectile quadrupole effects are treated explicitly in coupled channels calculations. The inelastic cross sections are dominated by the imaginary part of the transition form factor, but the deformation lengths still agree well with the experimental $B(EL)$ values for the $L = 2$, 3, and 5 transitions studied.

NUCLEAR REACTIONS ^{9}Be + ^{39}K, ^{40,44}Ca, $E = 40$ MeV; elastic and inelastic, ^{40}Ca(2^+, 3.90 MeV, 3^-, 3.74 MeV, and 5^-, 4.49 MeV) and ^{44}Ca(2^+, 1.16 MeV). Measured $\sigma(\theta)$ up to $\theta_{c.m.} = 120°$ and at $\theta_{c.m.} = 173.8°$. Double-folding model analysis, DWBA, deduced nuclear deformation lengths.

I. INTRODUCTION

The scattering of ^{9}Be projectiles has received considerable attention recently.[1-4] The absorption in ^{9}Be elastic scattering was found to be appreciably stronger than the absorption of other projectiles of a similar mass,[1-3] while inelastic ^{9}Be scattering was found to be dominated by the imaginary part of the transition form factor.[4] In the context of the double-folding model,[5] ^{9}Be elastic scattering appears to be anomalous,[3,6] as the $M3Y$ effective nucleon-nucleon interaction[7] has to be substantially reduced (by a factor of 2—3) to reproduce ^{9}Be elastic scattering data. The very weak binding energy of the ^{9}Be nucleus suggests itself as a natural explanation of the strong absorption in ^{9}Be elastic scattering,[2] and also of the ^{9}Be anomaly in the double-folding model.[6] However, a recent study[8] of quadrupole effects in ^{7}Li and ^{9}Be scattering demonstrated that the large static quadrupole moments of these nuclei play an important role in the scattering process. When the strong quadrupole effects in ^{9}Be + ^{40}Ca elastic scattering at $E_{lab} = 40$ MeV were treated explicitly in coupled channels calculations, no renormalization of the real double-folded potential, obtained with the $M3Y$ effective interaction, was needed to reproduce the data.[8]

In the present work, we report a measurement of extensive angular distributions for ^{9}Be + ^{39}K and ^{9}Be + ^{44}Ca elastic scattering at $E_{lab} = 40$ MeV, which complete the 40 MeV data for ^{9}Be + ^{40}Ca already reported in Ref. 8. These measurements were undertaken to determine the mass dependence of the effective nucleon-nucleon interaction and to search for the existence of anomalous large angle scattering as observed in ^{6}Li + ^{39}K, ^{40}Ca scattering. Together with the elastic cross sections, angular distributions for inelastic scattering of ^{9}Be leading to the first 2^+, 3^-, and 5^- states in ^{40}Ca, and to the first 2^+ state in ^{44}Ca are also presented. Both the elastic and inelastic scattering data were analyzed in terms of the double-folding model. The importance of higher-order effects, in particular the effect of the quadrupole moment of ^{9}Be, was investigated in coupled channels calculations.

II. EXPERIMENTAL PROCEDURE AND RESULTS

The ^{9}Be beam was produced in the form of BeH^- by flowing ammonia onto a ^{9}Be cone in an

inverted sputter source,[9] and accelerated by the Florida State University super FN tandem Van de Graaff accelerator. Beam currents of up to 300 nA of $^9Be^{4+}$ on target were obtained. The targets were prepared by vacuum evaporation of the target material onto carbon foils ($\sim 34\ \mu g/cm^2$, thick), and were transferred to the scattering chamber without breaking the vacuum. Natural KF ($\sim 100\ \mu g/cm^2$), natural metallic Ca ($\sim 100\ \mu g/cm^2$), and enriched ^{44}Ca (98.6%, $\sim 300\ \mu g/cm^2$) were used. An array of six Si surface barrier detectors mounted 10° apart in a 46 cm diam scattering chamber detected the scattered ions. Single detectors with an angular acceptance of 0.3° were employed in the four forward-angle positions, while ΔE-E telescopes (0.7° angular acceptance) were used in the last two positions to eliminate light reaction products at backward angles. A monitor detector at a small forward angle was used for normalization between runs.

Absolute normalization of the cross sections was established by measuring the elastic scattering of 25 MeV $^{12}C^{4+}$ ions from each of the targets, and assuming the scattering to be Rutherford. The absolute certainty in the normalization is estimated to be $\pm 6\%$.

The measured elastic angular distributions are shown in Fig. 1, and the inelastic cross sections are shown in Fig. 2. The error bars shown are due to counting statistics and uncertainties in peak fitting, and do not include the absolute error. The angular distributions for $^9Be + {}^{40}Ca$ and $^9Be + {}^{39}K$ elastic scattering extend to a ratio-to-Rutherford of $\sigma/\sigma_R \simeq 10^{-5}$ ($\theta_{c.m.} \simeq 120°$). The elastic cross sections have little structure and fall off exponentially in the whole angular range measured. There are some gaps in the inelastic angular distributions, which are due to difficulties in separating the yields from carbon or oxygen contaminant peaks.

A counter telescope was placed at a laboratory angle of 173° to determine the elastic cross section at this angle on each of the targets. To calibrate the detector, a ^9Be beam was scattered from an Au target. The ^9Be beam energy was chosen so that the scattered particles had the same energy as that expected from the K and Ca targets of interest.

III. ELASTIC SCATTERING ANALYSIS

The elastic scattering data were analyzed in terms of the double-folding model.[5] The real double-folded potential was obtained by evaluating

$$U(\vec{R}) = N \int d\vec{r}_p \int d\vec{r}_t \rho_p(\vec{r}_p)\rho_t(\vec{r}_t) \times V(|\vec{r}_p - \vec{r}_t + \vec{R}|) \quad (1)$$

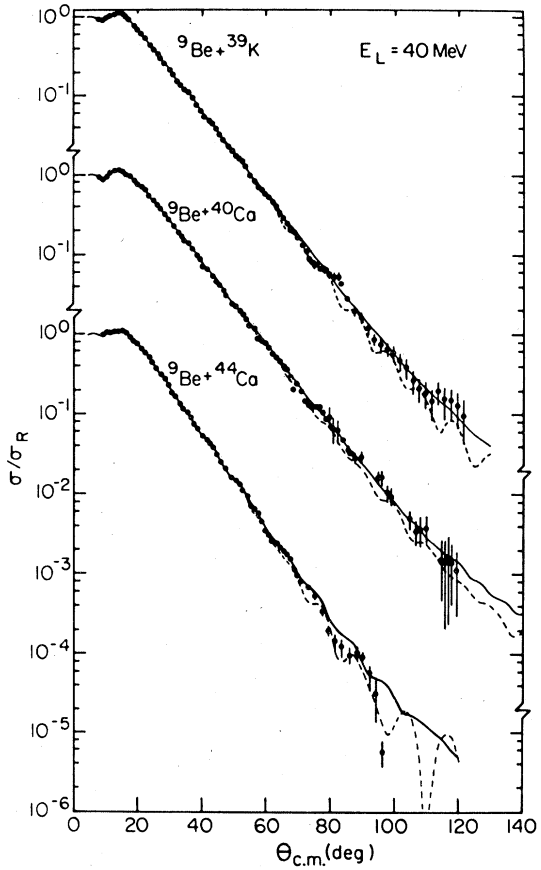

FIG. 1. Angular distributions for elastic scattering of $^9Be + {}^{39}K$, $^9Be + {}^{40}Ca$, and $^9Be + {}^{44}Ca$ at $E_{lab} = 40$ MeV, compared with the double-folding model fits. The dashed lines are calculations without quadrupole effects when N was allowed to vary, and the solid lines are results of the coupled channel calculations with N fixed at 1.0.

using momentum-space techniques.[10] Here $\rho_{p,t}(\vec{r}_{p,t})$ is the point nucleon density of the projectile or target nucleus measured with respect to its center of mass, and $\vec{R}$ is the separation of the two colliding nuclei. The effective nucleon-nucleon interaction V was the $M3Y$ interaction of Bertsch *et al.*,[7] which is based on a realistic G matrix, modified to account for single-nucleon knockout exchange (SNKE).[11] Only the $S = T = 0$ term was used, of the explicit form (energies in MeV and lengths in fm)

$$V(r) = 7999\frac{e^{-4r}}{4r} - 2134\frac{e^{-2.5r}}{2.5r} - 3918(\vec{r}), \quad (2)$$

where the δ-function term approximates SNKE in

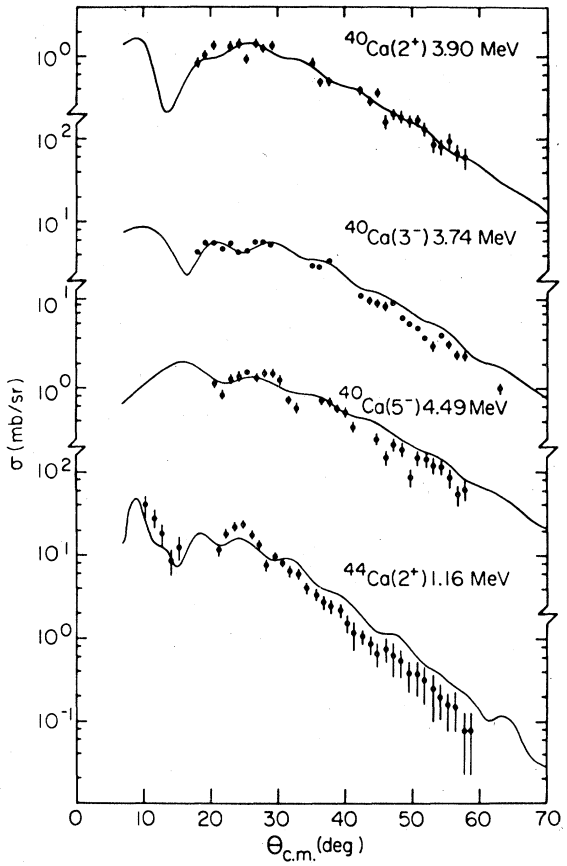

FIG. 2. Angular distributions for inelastic scattering of ^{9}Be + ^{40}Ca and ^{9}Be + ^{44}Ca at $E_{lab} = 40$ MeV, leading to the first 2^+, 3^-, and 5^- states in ^{40}Ca, and the first 2^+ state in ^{44}Ca. The solid lines are DWBA fits to the data.

this energy range. The factor N in Eq. (1) is a renormalization of the real double-folded potential, which was varied to obtain the best fit to the data. If the model is correct, then $N \simeq 1.0$. The imaginary part of the optical potential had the conventional Woods-Saxon form, whose radius parameter was kept fixed at $r_I = 1.22$ fm while the depth and diffuseness were adjusted.

The proton parts of the densities of the ^{9}Be projectile and the targets were taken from electron elastic scattering work.[12] The neutron part of the ^{9}Be density was derived from the proton part by adjusting the harmonic oscillator parameter so that the difference between the neutron and proton rms radii, after a deconvolution of the proton size, was 0.38 fm (method B of Ref. 6). The neutron parts of the target densities were obtained by assuming a neutron skin predicted by the droplet model.[13] The parameters of the densities used are given in Table I. The proton size was deconvoluted from these densities during the momentum-space evaluation of the integral in Eq. (1).

The best fits to the elastic cross section data obtained with this procedure are shown in Fig. 1 (dashed curves), and the corresponding potential parameters are given in Table II. A renormalization of the real double-folded potential by a factor $N \simeq 0.6$ was needed to fit the ^{9}Be elastic scattering data for all three targets. This renormalization is substantial, but not as drastic as the factor $N \simeq 0.3$ reported recently[3] for ^{9}Be + ^{40}Ca at 45 and 60 MeV.

The ^{9}Be nucleus has a large static quadrupole moment, $Q_2 = 4.9 \pm 0.3$ e fm^2,[14] which is neglected when only a spherical density is used. We studied the effects of the quadrupole moment by adding a quadrupole term to the spherical density of ^{9}Be:

$$\rho(\vec{r}) = \rho_0(r) + \rho_2(r) Y_{20}(\hat{r}) \ . \tag{3}$$

Here the body fixed coordinate system is used, $\rho_0(r)$ is the spherical density of ^{9}Be given by Table I, and $\rho_2(r)$ is the quadrupole density. For simplicity, the quadrupole density was given a derivative form

$$\rho_2(r) = \delta_2 \frac{d\rho_0(r)}{dr} \ , \tag{4}$$

where δ_2 is the quadrupole deformation length. The

TABLE I. Parameters of the projectile and target densities. The ^{9}Be density has the form $\rho(r) = (A + BC^2r^2)\exp(-C^2r^2) + (D + EF^2r^2)\exp(-F^2r^2)$, and the target densities are $\rho(r) = A/\{1 + \exp[(r - B)/C]\} + D/\{1 + \exp[(r - E)/F]\}$. The densities are given in units of fm^{-3}.

Nucleus	A	B	C	D	E	F
^{9}Be	0.0651	0.0398	0.5580	0.0544	0.0332	0.4878
^{39}K	0.083 74	3.521	0.550	0.086 76	3.5425	0.550
^{40}Ca	0.0849	3.572	0.550	0.0858	3.558	0.550
^{44}Ca	0.0802	3.651	0.550	0.0888	3.763	0.550

TABLE II. Optical potential parameters. The potential has a double-folded real part, renormalized by the factor N, and a Woods-Saxon imaginary part. The projectile quadrupole deformation length δ_2 was used in the coupled channel calculations, in which N was fixed at 1.0.

System	N	W (MeV)	a_I (fm)	δ_2 (fm)	$L_{1/2}(\hbar)$	$D_{1/2}$ (fm)	$U_{1/2}$ (MeV)	$W_{1/2}$ (MeV)
^{9}Be + ^{39}K	0.75	23.4	0.74	0	23.9	9.1	0.73	0.88
	1.0	32.0	0.71	2.5	25.1	9.1	0.98	1.05
^{9}Be + ^{40}Ca	0.66	22.9	0.71	0	24.0	9.1	0.68	0.79
	1.0	35.0	0.71	2.5	25.1	9.1	1.03	1.21
^{9}Be + ^{44}Ca	0.56	16.4	0.84	0	25.5	9.3	0.53	0.88
	1.0	24.0	0.70	2.5	25.4	9.3	0.95	0.71

$R_I = 1.22(A_p^{1/3} + A_t^{1/3})$; $R_c = 1.3A_t^{1/3}$ fm; $D_{1/2} = 1.66(A_p^{1/3} + A_t^{1/3})$

parameter δ_2 was fixed by normalizing the quadrupole density to the intrinsic electric quadrupole moment Q_{20} of ^{9}Be:

$$\left[\frac{16\pi}{5}\right]^{1/2} \int_0^\infty \rho_2(r) r^4 dr = \frac{A}{Ze} Q_{20} . \quad (5)$$

This seemed to be the simplest procedure, in view of the absence of a model-independent knowledge of the deformation of the neutron distribution. The rotational model was assumed with $K = I = \frac{3}{2}^-$ for the ground state of ^{9}Be, and thus the intrinsic moment Q_{20} is given by $Q_{20} = 5Q_2 = 25\ e\ \text{fm}^2$ with the experimental value[14] of the static moment Q_2. This procedure resulted in a value $\delta_2 = 2.5$ fm for the quadrupole deformation length. The use of the deformed density (3) in the folding integral (1) generated a quadrupole term in the real double-folded potential, in addition to the monopole term. As the quadrupole density $\rho_2(r)$ is derived from a spherical density which is not corrected for the finite proton size, the proton size was unfolded from $\rho_2(r)$ during the evaluation of the double-folded quadrupole term. An imaginary quadrupole term of a derivative Woods-Saxon form, with the same deformation length as for the real part, was also included in the optical potential.

Coupled channels calculations were carried out for the ^{9}Be elastic scattering from ^{40}Ca, ^{44}Ca, and ^{39}K, using the quadrupole term in the optical potential to couple the ground state of ^{9}Be to itself (reorientation coupling). A modified version of the coupled channels code CHUCK[15] was employed in these calculations. The renormalization factor was fixed at $N = 1.0$, but the depth W of the imaginary Woods-Saxon potential was varied to adjust for the coupling effects. The results of the coupled channel calculations are shown in Fig. 1 (solid curves). It can be seen that the data are fitted at least as well as in the calculations without quadrupole effects, and thus the need to renormalize the real double-folded potential is removed (N was fixed at 1.0). This result indicates that the $N \sim 0.6$ renormalization, needed when only a spherical double-folded potential was used, simulates the strong quadrupole effects in ^{9}Be elastic scattering. The potential parameters used in the coupled channel calculations are summarized in Table II.

The coupling effect due to the excitation of the $\frac{5}{2}^-$ (2.43 MeV) state in ^{9}Be is difficult to assess, as it is not possible to observe the ^{9}Be projectile excitation in the detection setup we used, and for this reason it was not included in the calculations. An explicit treatment of the effects due to the excitation of the target states together with the projectile quadrupole effects was not attempted due to the computational complexity of the problem. In any case, coupled channels calculations which did not include the projectile quadrupole effects showed that the excited states of the ^{40}Ca and ^{44}Ca targets, which are of a vibrational character, played a minor role in influencing the elastic cross sections.

IV. INELASTIC SCATTERING ANALYSIS

The double-folding model was also employed to analyze the measured inelastic cross sections for the excitation of the first 2^+, 3^-, and 5^- in ^{40}Ca and the first 2^+ state in ^{44}Ca. A 2^L-pole deformation of the density of the nucleus excited leads to a real double-folded form factor for inelastic excitation of multipolarity L; this is a natural extension of the folding model to inelastic scattering to collective states.[5,16] As in the investigation of the projectile quadrupole effects, a derivative form was assumed for the 2^L-pole transition densities $\rho_L(r)$:

$$\rho_L(r) = \delta_L \frac{d\rho_0}{dr} , \quad (6)$$

where $\rho_0(r)$ is the spherical density of the target, and δ_L is the 2^L-pole nuclear deformation length for the inelastic transition. When the equivalence of the charge and nuclear transition density $\rho_L(r)$ is related to the reduced electric transition probability $B(EL;0\rightarrow L)$ as

$$\int_0^\infty \rho_L(r) r^{L+2} dr = \frac{A}{Ze}[B(EL)]^{1/2} . \quad (7)$$

With the form (6) for the transition densities, Eq. (7) simply sets the charge and nuclear deformation lengths equal, when the proton and neutron spherical densities have the same shape. The experimental $B(EL)$ values[17–19] for the transitions considered here, and the deformation lengths δ_L derived using Eqs. (6) and (7) and the spherical target densities of Table I, are given in Table III.

The inelastic cross sections were calculated in the distorted-wave Born approximation (DWBA). The distorted waves were generated with the double-folded real and Woods-Saxon imaginary potentials which fitted the elastic data in the calculations without projectile quadrupole effects (see Sec. III). These effects were simulated by the renormalization of the real double-folded potential. The real double-folded form factors were renormalized in the same way as the real potentials. The imaginary part of the transition form factor had the conventional, Woods-Saxon derivative form with the same deformation length as used in the real part.

Coulomb excitation was included using the $B(EL)$ values of Table III, but was found to be important only for the quadrupole excitations, where 400 partial waves were included using the method of Samuel and Smilansky[20] for the high partial waves. The nuclear deformation lengths δ_L were adjusted to the magnitude of the inelastic cross sections, and are compared with the deformation lengths derived from the $B(EL)$ values in Table III. The DWBA fits are shown in Fig. 2 (solid lines). As can be seen, the inelastic angular distributions are reproduced quite well.

The real part of the transition form factor contributes relatively very little to the inelastic cross sections, as setting the imaginary part to zero reduced the cross sections by almost a factor of 10; this makes inelastic ^{9}Be scattering quite insensitive to the details of the real transition form factor. The inelastic cross sections are thus dominated by the phenomenological imaginary form factor; and it is, therefore, rather surprising that the deformation lengths found by fitting the data agree so well with the $B(EL)$ values (see Table III). In fact, the δ_L values for the $L = 2$ and 3 transitions in ^{40}Ca are in excellent agreement (equal within errors) with the results of a recent double-folding model analysis[21] of ^{11}B + ^{40}Ca inelastic scattering at 51.5 MeV, where the real part of the transition form factor was dominant. Here, as in the case of ^{11}B + ^{40}Ca, higher order effects were not needed to describe the inelastic scattering, in contrast to ^{16}O + ^{40}Ca at 60 MeV, where the 5^- transition could only be fitted with coupled channels calculations.[22]

V. LARGE ANGLE CROSS SECTIONS

One motivation of this study was to determine whether ^{9}Be scattering had enhanced large angle cross sections like those observed[23] for ^{6}Li + ^{39}K,

TABLE III. Deformation lengths for inelastic transitions in the ^{9}Be + ^{40}Ca and ^{9}Be + ^{44}Ca systems.

Transition	Q (MeV)	L	$B(EL)$ (e^2fm^{2L})	δ_L[a] (fm)	δ_L[b] (fm)	δ_L[c] (fm)
$0^+ \rightarrow 2^+$(^{40}Ca)	−3.90	2	90[d]	0.46	0.44	0.44
$0^+ \rightarrow 3^-$(^{40}Ca)	−3.74	3	1.5×10^4[d]	1.30	1.15	1.15
$0^+ \rightarrow 5^-$(^{40}Ca)	−4.49	5	3×10^6[e]	0.75	1.00	0.81
$0^+ \rightarrow 2^+$(^{44}Ca)	−1.16	2	470[f]	1.02		1.02

[a]Derived from the $B(EL)$ values using Eq. (7).
[b]Reference 21.
[c]Found by fitting the present data.
[d]Reference 17.
[e]Reference 18.
[f]Reference 19.

^{40}Ca. For ^{6}Li + ^{39}K at a bombarding energy of 34 MeV, the value of $\sigma/\sigma_R = 1.3 \pm 0.13 \times 10^{-3}$ at $\theta_{\text{c.m.}} = 173.3°$. In the present work, for a bombarding energy of 40 MeV at $\theta_{\text{c.m.}} = 173.9°$, $\sigma/\sigma_R = 1.0 \pm 0.3 \times 10^{-4}$ for ^{9}Be + ^{39}K, and $1.9 \pm 0.3 \times 10^{-4}$ for ^{9}Be + ^{40}Ca. These results, taken with the results of Ref. 23, seem to indicate that both ^{7}Li and ^{9}Be do not have enhanced large angle cross sections, implying that the phenomenon is not related to the small binding energy of the ^{6}Li, ^{7}Li, and ^{9}Be projectiles. However, this tentative conclusion should be treated with caution, because of the possible oscillatory nature of the angular distributions at large angles. The data are a factor of 10 larger than the calculated cross sections at this angle.

VI. CONCLUSIONS

Elastic scattering of ^{9}Be by ^{40}Ca, ^{44}Ca, and ^{39}K was studied at $E_{\text{lab}} = 40$ MeV, together with ^{9}Be inelastic scattering leading to the lowest 2^+, 3^-, and 5^- states in ^{40}Ca and the lowest 2^+ state in ^{44}Ca. The measured elastic angular distributions, which cover an extensive angular range (up to $\theta_{\text{c.m.}} \simeq 120°$), are characteristic of strong absorption, with no backward-angle enhancement.

Both the elastic and inelastic data were analyzed in terms of the double-folding model with a realistic effective nucleon-nucleon interaction.[7] The need to renormalize the effective nucleon-nucleon interaction by a factor of about 0.6 was shown to be related to the large static quadrupole moment of ^{9}Be, as the elastic cross sections could be fitted without renormalization ($N = 1.0$) when the strong quadrupole effects were treated explicitly in coupled channels calculations.

Quadrupole effects undoubtedly play an important role in the recently studied elastic scattering of ^{9}Be by ^{28}Si at 121 and 201.6 MeV (Ref. 2), where, however, coupling effects due to the strongly-excited states in ^{28}Si could complicate the picture. Unfortunately, coupled channels calcultions, in which both the projectile and target higher-order effects are included, still impose an excessive demand on the computing time, especially when a large number of partial waves is required.

The inelastic scattering of ^{9}Be + ^{40}Ca and ^{9}Be + ^{44}Ca was described well by DWBA calculations, using real double-folding potentials and transition form factors, renormalized to simulate the projectile quadrupole effects. The imaginary part of the transition form factor dominates the inelastic cross section, so the analysis was not sensitive to the real double-folded form factors. The deformation lengths δ_L found by fitting the inelastic data thus reflect chiefly the deformation of the imaginary Woods-Saxon potential. For this reason, the very good agreement for all multipolarities ($L = 2$, 3, and 5) between the deformation lengths derived from the $B(EL)$ values and the values of δ_L which fitted the data is quite surprising.

ACKNOWLEDGMENTS

This work was supported in part by the National Science Foundation. One of the authors (V.H.) gratefully acknowledges the support of the Florida State University and the Council for Scientific and Industrial Research, Pretoria. The authors wish to acknowledge constructive discussions with C. W. Glover, F. Petrovich, D. Robson, and D. Stanley.

*On leave of absence from the Department of Physics, University of the Witwatersrand, Johannesburg, South Africa.

[1]R. Balzer, M. Hugi, B. Kamys, J. Lang, R. Müller, E. Ungricht, J. Unternährer, L. Jarczyk, and A. Strzalkowski, Nucl. Phys. A293, 518 (1977).
[2]M. S. Zisman, J. C. Cramer, D. A. Goldberg, J. W. Watson, and R. M. DeVries, Phys. Rev. C 21, 2398 (1980).
[3]J. S. Eck, T. R. Ophel, P. D. Clark, and D. C. Weisser, Nucl. Phys. A334, 519 (1980).
[4]J. S. Eck, T. R. Ophel, P. D. Clark, and D. C. Weisser, Nucl. Phys. A341, 178 (1980).
[5]G. R. Satchler and W. G. Love, Phys. Rep. 55, 185 (1979).
[6]G. R. Satchler, Phys. Lett 83B, 284 (1979).
[7]G. Bertsch, J. Borysowicz, H. McManus, and W. G. Love, Nucl. Phys. A284, 399 (1977).
[8]V. Hnizdo, K. W. Kemper, and J. Szymakowski, Phys. Rev. Lett. 46, 590 (1981).
[9]K. R. Chapman, Nucl. Instrum. Methods, 124, 229 (1975); R. I. Cutler, K. W. Kemper, and K. R. Chapman, Nucl. Instrum. Methods 164, 605 (1979).
[10]F. Petrovich, Nucl. Phys. A251, 143 (1975); F. Petrovich and D. Stanley, *ibid.* A275, 487 (1977).
[11]M. Golin, F. Petrovich, and D. Robson, Phys. Lett. 64B, 253 (1976).
[12]C. W. deJager, H. deVries, and C. deVries, At. Data Nucl. Data Tables 14, 479 (1974).
[13]W. D. Myers, Nucl. Phys. A145, 387 (1970).

[14]A. G. Balchman and A. Lurio, Phys. Rev. 153, 164 (1967).
[15]P. D. Kunz (unpublished).
[16]P. V. Moffa, C. B. Dover, and J. P. Vary, Phys. Rev. C 16, 1857 (1977).
[17]P. L. Hallowell, W. Bertozzi, J. Heisenberg, S. Kowalski, X. Maruyama, C. P. Sargent, W. Turchinetz, and C. F. Williamson, Phys. Rev. C 7, 1396 (1973).
[18]J. Heisenberg, J. S. McCarthy, and I. Sick, Nucl. Phys. A164, 353 (1971).
[19]C. W. Towsley, D. Cline, and R. N. Horoshko, Nucl. Phys. A204, 574 (1973).
[20]M. Samuel and U. Smilansky, Comput. Phys. Commun. 2, 445 (1971).
[21]V. Hnizdo, C. W. Glover, and K. W. Kemper, Phys. Rev. C 23, 236 (1981).
[22]K. E. Rehm, W. Henning, J. R. Erskine, and D. G. Kovar, Phys. Rev. Lett. 40, 1479 (1978).
[23]R. I. Cutler, M. J. Nadworny, and K. W. Kemper, Phys. Rev. C 15, 1318 (1977); H. Bohn, K. A. Eberhard, R. Vandenbosch, K. G. Bernhardt, R. Bangert, and Y-d Chan, *ibid.* 16, 665 (1977); J. Szymakowski, K. W. Kemper, and A. D. Frawley, Nucl. Phys. A355, 221 (1981).